



HAL
open science

Molecular dynamics simulation of the capillary leveling of a glass-forming liquid

Ioannis Tanis, Konstantinos Karatasos, Thomas Salez

► **To cite this version:**

Ioannis Tanis, Konstantinos Karatasos, Thomas Salez. Molecular dynamics simulation of the capillary leveling of a glass-forming liquid. 2019. hal-01909064v3

HAL Id: hal-01909064

<https://hal.science/hal-01909064v3>

Preprint submitted on 28 Aug 2019 (v3), last revised 16 Sep 2019 (v4)

HAL is a multi-disciplinary open access archive for the deposit and dissemination of scientific research documents, whether they are published or not. The documents may come from teaching and research institutions in France or abroad, or from public or private research centers.

L'archive ouverte pluridisciplinaire **HAL**, est destinée au dépôt et à la diffusion de documents scientifiques de niveau recherche, publiés ou non, émanant des établissements d'enseignement et de recherche français ou étrangers, des laboratoires publics ou privés.

1 **Molecular Dynamics Simulation of the Capillary Leveling of**
2 **a Glass-Forming Liquid**

3
4 Ioannis Tanis^{1*}, Kostas Karatasos^{2,3}, Thomas Salez^{4,5}

5
6 ¹Laboratoire de Physico-Chimie Théorique, UMR CNRS Gulliver 7083,
7 ESPCI Paris, PSL Research University, 75005 Paris, France

8 ²Laboratory of Physical Chemistry, Department of Chemical Engineering, Aristotle
9 University of Thessaloniki, 54124, Thessaloniki

10 ³Institute of Electronic Structure and Laser, Foundation for Research and Technology
11 - Hellas, P. O. Box 1527, 711 10 Heraklion Crete, Greece

12 ⁴Univ. Bordeaux, CNRS, LOMA, UMR 5798, F-33405, Talence, France

13 ⁵Global Station for Soft Matter, Global Institution for Collaborative Research and
14 Education,

15 Hokkaido University, Sapporo, Hokkaido 060-0808, Japan
16
17
18
19
20
21
22
23
24
25
26
27
28
29
30
31

32 * Corresponding author e-mail address: tanis.ioannis@gmail.com

33 **Abstract.** Motivated by recent experimental studies probing i) the existence of a
34 mobile layer at the free surface of glasses, and ii) the capillary leveling of polymer
35 nanofilms, we study the evolution of square-wave patterns at the free surface of a
36 generic glass-forming binary Lennard-Jones mixture over a wide temperature range,
37 by means of molecular dynamics simulations. The pattern's amplitude is monitored
38 and the associated decay rate is extracted. The evolution of the latter as a function of
39 temperature exhibits a crossover between two distinct behaviours, over a temperature
40 range typically bounded by the glass-transition temperature and the mode-coupling
41 critical temperature. Layer-resolved analysis of the film particles' mean-squared
42 displacements further shows that diffusion at the surface is considerably faster than in
43 the bulk, below the glass-transition temperature. The diffusion coefficient of the
44 surface particles is larger than its bulk counterpart by a factor that reaches 10^5 at the
45 lowest temperature studied. This factor decreases upon heating, in agreement with
46 recent experimental studies.

47
48
49
50
51
52
53
54
55
56
57
58
59
60
61
62
63
64
65
66

67 **I. Introduction**

68 Thin films and their free interfaces are used in a variety of applications such as
69 catalysis¹, fast crystal growth^{2, 3} and the formation of low-energy glasses^{4, 5}. Apart
70 from their applications in industry and technology, molecular mobility and relaxation
71 at surfaces and interfaces have been recently a subject of growing interest for
72 fundamental research. To this end, several experimental approaches have been used to
73 probe the surface evolution and mobility of thin films⁶⁻¹⁰. More specifically, an
74 efficient way to gain insight into the surface mass transport and the associated
75 dynamics, is to deposit nanoparticles on the film surface and subsequently to monitor
76 the host material's response^{9,11}. Another powerful and versatile technique widely
77 utilized for the determination of the surface-diffusion coefficient D_s , characterizing
78 the in-plane translation of molecules at the film surface, is the capillary-driven
79 leveling of surface-gratings^{6, 9, 12-14}. Several studies suggest that the mechanism
80 governing the relaxation of these gratings is temperature and material dependent^{12, 15}.
81 More specifically, recent works on glass-forming molecular liquids reported a
82 transition from bulk viscous flow at temperatures higher than the glass-transition
83 temperature T_g , to surface diffusion below T_g ^{13, 16}. Analogous studies in polymeric
84 liquids revealed that bulk viscous flow was the only mechanism governing the surface
85 decay, even at the highest viscosities studied^{14, 17, 18}. According to Mullin's pioneering
86 work¹⁹, the different mechanisms that could flatten the surface pattern (surface and
87 bulk diffusions, evaporation-condensation, bulk viscous flow) can be distinguished by
88 determining the decay rate dependence on spatial frequency. This method has been
89 applied in crystalline metals²⁰, amorphous silica²¹ and molecular glasses²².
90 Measurements of diffusion coefficients at the surface report values considerably
91 higher than the respective bulk coefficients at the glass-transition temperature^{12,13}.
92 Furthermore, large variations in surface diffusion coefficients among different
93 molecular glass formers bearing a similar bulk mobility were linked to the strength of
94 the intermolecular forces²³.
95 Further insight into glass-forming systems has been provided by numerical
96 simulations. Several studies have addressed the factors that govern dynamical
97 heterogeneity and spatial correlations in the bulk²⁴⁻³⁰. Furthermore, other works
98 addressing systems under confinement have managed to elucidate the effects of
99 confinement by rough or smooth walls on the liquid dynamics and to extract
100 associated length-scales³¹⁻³⁵. Extensive simulation studies have also been conducted

101 on ultrastable vapor-deposited glasses^{4, 36, 37}. However, to our knowledge, a small
102 number of simulation studies probing the surface mobility in glass formers have been
103 reported so far.

104 Surface-diffusion-mediated decay of two-dimensional nanostructures has been
105 recently studied by a combined analytical and kinetic Monte-Carlo approach³⁸,
106 whereas Kayhani *et al.* performed molecular dynamics (MD) simulations to examine
107 the coalescence of platinum nanoclusters³⁹. Concerning simulation work on the
108 surface mobility of molecular glass formers, Hoang *et al.* performed MD studies on
109 freestanding monatomic glass-forming liquids⁴⁰. The study of Akbari *et al.* addressed
110 the effects of the substrate in kinetic and thermodynamic properties of a binary
111 Lennard-Jones (LJ) liquid⁴¹, whereas Malshe and co-workers extracted surface-
112 diffusion coefficients by the aid of the grating-decay approach⁴² in free standing films
113 of the aforementioned liquid type. Results were consistent with data obtained from the
114 mean-squared displacements of the liquid particles. In a very recent study, Kuan and
115 co-workers examined single-particle dynamics in the surface and in the bulk of
116 supported films prepared by vapour deposition. Both bulk and surface particle
117 displacements showed evidence of heterogeneous dynamics⁴³.

118 The aim of the present work is to provide additional insight into the surface mobility
119 of a glass-forming liquid by means of molecular dynamics simulations. Similarly to a
120 recent work where we probed the viscoelastic behaviour of nonentangled polymer
121 films above the glass-transition temperature, through the capillary leveling of a
122 square-wave surface pattern⁴⁴, we examine here the evolution of a square-wave
123 surface pattern atop a generic binary LJ mixture supported by an attractive substrate.
124 This new study is carried out over a wide temperature range, sampling both the glassy
125 and liquid states of the film. The associated decay rates are extracted whereas surface
126 and bulk mobilities are examined. Further insight into the surface and bulk mobilities
127 is gained by examining the self part of the van Hove function, as well as via the layer-
128 resolved analysis of the liquid particles' mean-squared displacements.

129

130 **II. Computational Details**

131 We examine a binary mixture of 80% A and 20% B particles that interact via a LJ
132 potential $V_{\alpha\beta} = 4\epsilon_{\alpha\beta} \left[(\sigma_{\alpha\beta}/r)^{12} - (\sigma_{\alpha\beta}/r)^6 \right]$, ($\alpha, \beta \in \{A, B\}$). The Van der Waals
133 parameters were chosen as $\epsilon_{AA} = 1.0, \sigma_{AA} = 1.0, \epsilon_{AB} = 1.5, \sigma_{AB} = 0.8, \epsilon_{BB} =$

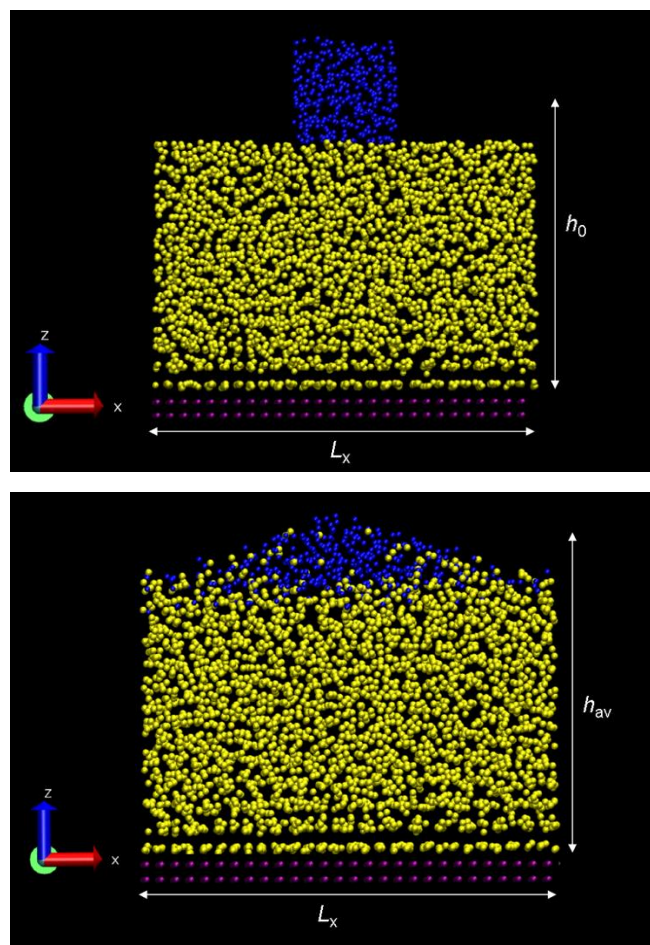
134 $0.5, \sigma_{BB} = 0.88$. The potential was truncated at a cut-off radius $r_c = 2.5\sigma_{AB}$. The
 135 numbers of particles of type A and B are 2938 and 734, respectively. The binary
 136 mixture interacting with this parameter set corresponds to the Kob-Andersen liquid
 137 model which is not prone to crystallization or to phase separation; it is extensively
 138 utilized in studies of glass-forming liquids^{45, 46}. The liquid film is supported by a
 139 strongly attractive substrate whose atoms (henceforth designated by the type S) are
 140 located on the sites of an hexagonal lattice and are kept fixed to their lattice positions.
 141 The substrate particles' radius is $\sigma_S = 2.41$ and they attract A and B atoms with the
 142 following energy magnitudes⁴⁷: $\epsilon_{AS} = 4.425$ and $\epsilon_{BS} = 3.129$. The length of the
 143 cubic box is $16.56\sigma_{AA}$ in the lateral directions x and y , and $441.17\sigma_{AA}$ in the z
 144 dimension. The value of the latter is chosen large enough to avoid interaction of the
 145 particles with periodic images of the substrate, and ensure a system pressure $p = 0$. All
 146 quantities are reported in LJ units, *i.e.* length is measured in units of σ_{AA} , energy in
 147 units of ϵ_{AA} , time in units of $\tau = (m\sigma_{AA}^2/(48\epsilon_{AA}))^{1/2}$ and temperature in units of
 148 ϵ_{AA}/k_B where k_B stands for the Boltzmann constant. For the case of argon, these units
 149 correspond to a length of 3.4 \AA , an energy of $120Kk_B$ and a time of $3 \cdot 10^{-13} \text{ s}$. All
 150 simulations are performed in the canonical (NVT) ensemble using the DL_POLY
 151 code⁴⁸. Temperature is maintained constant through the use of the Nosé-Hoover
 152 thermostat. Simulations are conducted at the temperature range $T = 0.20-0.525$, and
 153 the length of each run is $3 \cdot 10^5$.

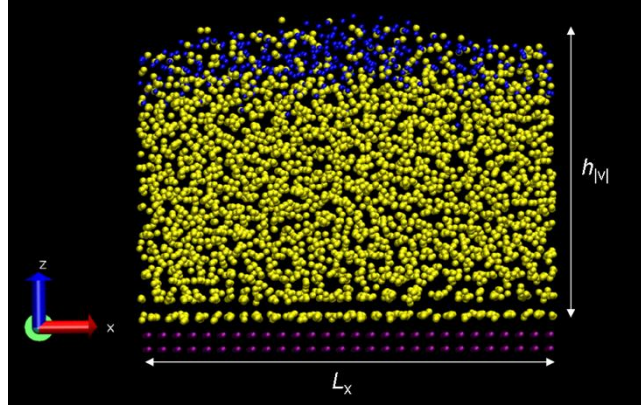
154 The initial configuration of the glassy film was obtained by the aid of the Aten
 155 program⁴⁹. To create the 3-dimensional pattern at the free surface of the film, a flat
 156 film was initially equilibrated in the canonical ensemble at a temperature of $T = 0.3$.
 157 Afterwards, particles were removed from both edges of the free surface in order to
 158 obtain the 3D pattern, henceforth designated as the 'top layer' (see Fig.1). The lateral
 159 dimensions of the latter were $L_x = L_y = 4.41$, whereas its thickness and initial height
 160 (counted from the substrate) were respectively $d = 4.36$ and $h_0 = 15.67$.

161 To examine the behaviour in the bulk, a configuration comprising 5076 particles was
 162 constructed at an elevated temperature, $T = 0.80$, and at a density of $\rho = 1.2$. After
 163 removing close contacts, the system was cooled to $T = 0.30$ by conducting runs in the
 164 isothermal-isobaric ensemble (NPT) at pressure $p = 0$. The temperature step between
 165 the isothermal runs ranged from $dT = 0.1$ for the highest temperatures to $dT = 0.025$
 166 and $dT = 0.0125$ at temperatures around the bulk glass-transition temperature T_g . The

167 duration of each isothermal run ranged from $1.6 \cdot 10^4$ (at $T > 0.5$) to $3 \cdot 10^5$ (at $T \leq 0.5$).
 168 Defining the cooling rate as the difference between the starting temperature and the
 169 final temperature divided by the time of the quench, the cooling rate was $0.75 \cdot 10^{-7}$.
 170 This amounts to half the cooling rate used in the original model of Kob and Andersen
 171 and, although it remains quite fast, it is slower than the fastest cooling rate in
 172 experiments⁴⁵. The glass-transition temperature of the binary mixture was determined
 173 by extrapolating and intersecting the affine dependencies of the low- and high-
 174 temperature specific-volume-vs-temperature curves. This yielded a value of $T_g =$
 175 0.392 which is below the reported mode-coupling critical temperature for this system,
 176 $T_c \approx 0.435$ ⁵⁰.
 177 Figure 1 displays the initial configuration of the samples, as well as snapshots from a
 178 run at $T = 0.3$ at times $t = 20000$ and 233333 . All snapshots were generated by the aid
 179 of the VMD software⁵¹. The particles that evaporated at elevated temperatures were
 180 disregarded from post-analysis.

181





182 Figure 1: Top: Initial configuration of the sample bearing a total number of 3672
 183 particles. Periodic boundary conditions are applied in all directions. L_x stands for the
 184 x -dimension of the simulation box and h_0 is the maximum vertical height (colour
 185 code : blue = top layer, yellow = bottom layer, purple = substrate). Middle: Snapshot
 186 of the film at $t = 20000$, where h_{av} is the average height value. Bottom: Snapshot of
 187 the film at $t = 233333$; h_{avl} the average height of the fully leveled film.

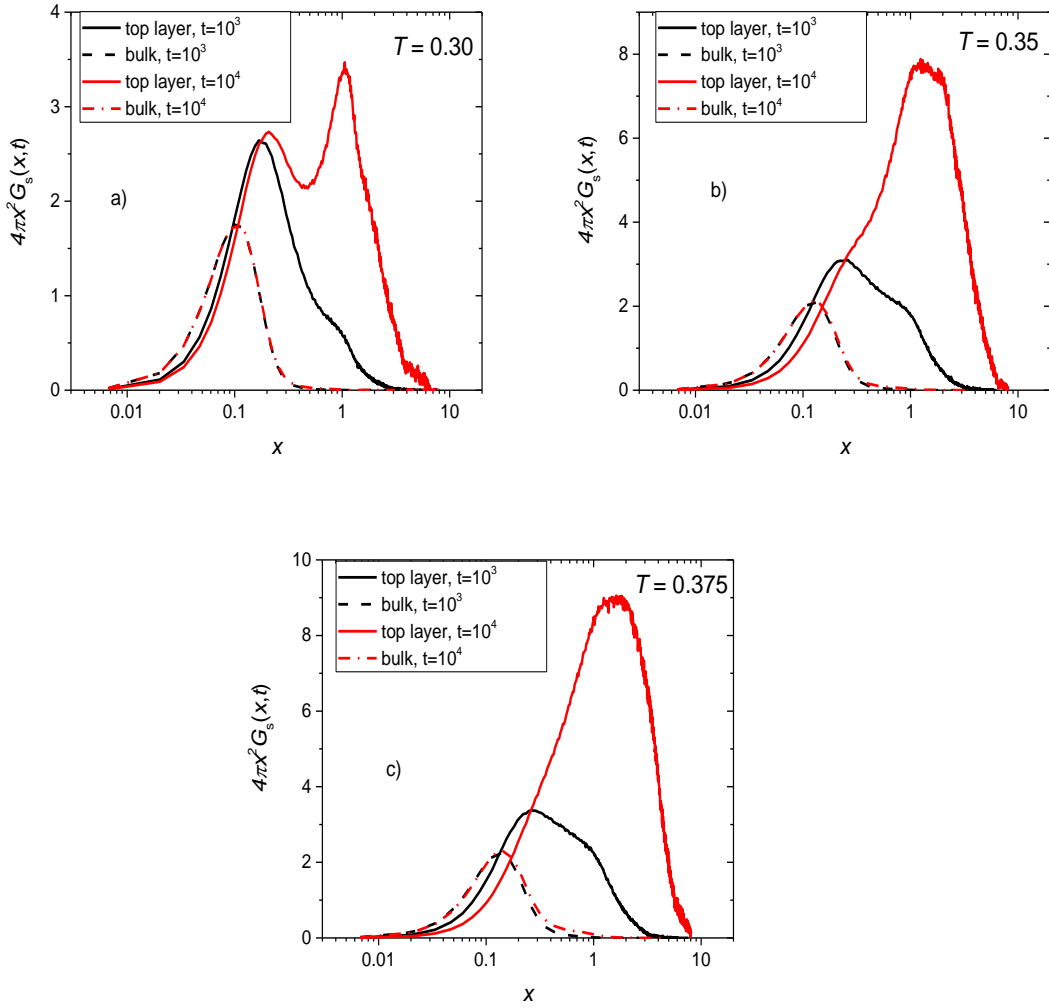
188

189 III. Results

190 To investigate the mobility of the liquid's molecules, we examine the self-part of the
 191 van Hove space-time correlation function defined as :

$$192 \quad G_s(x, t) = \frac{1}{N} \sum_{i=1}^N \langle \delta(x + x_i(0) - x_i(t)) \rangle, \quad (1)$$

193 with x_i representing the position of particle i along any of the x , y and z directions, N
 194 being the number of particles that constitute the top layer, $\langle \dots \rangle$ being the ensemble
 195 average over realizations and time origins and δ is the Dirac's distribution. In order to
 196 account for the natural anisotropy of the system induced by the interfaces, the van
 197 Hove function was evaluated in each direction separately. In Fig.2, the x dependencies
 198 of $4\pi x^2 G_s(x, t)$ for the top layer particles and two times t , are displayed. A
 199 practically indistinguishable behaviour (not shown for clarity reasons) was observed
 200 in the y direction, as well. Also shown in the figure, are the corresponding curves for
 201 the bulk sample. The van Hove functions were evaluated at the temperatures $T = 0.30$
 202 and $T = 0.35$, which lie below the bulk T_g as well as at a temperature $T = 0.375$ near
 203 the bulk T_g .



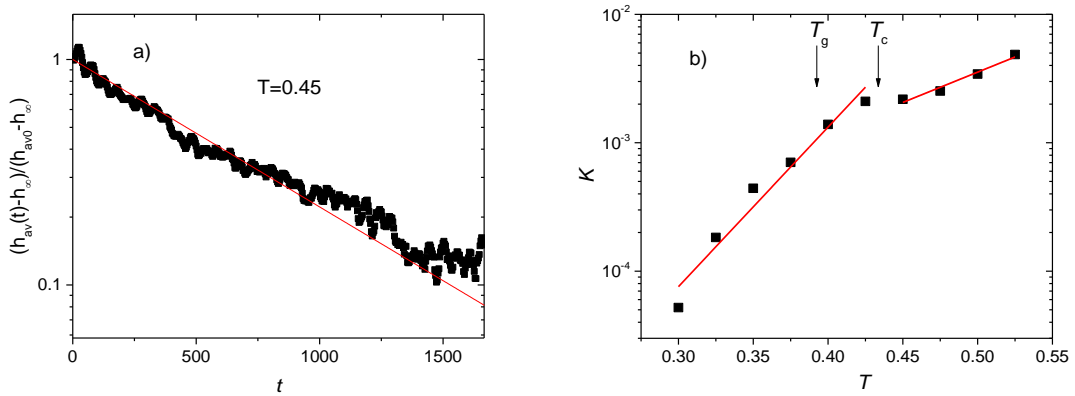
204 Figure 2: Self part of the van Hove function (eq.1) for the top layer particles, as a
 205 function of the molecular displacement in the x direction, evaluated at a) $T = 0.30$, b)
 206 $T = 0.35$ and c) $T = 0.375$. The different line colours correspond to different times and
 207 the references for a bulk sample are provided for comparison.

208

209 A visual inspection of Fig.2 reveals that the top layer particles are significantly more
 210 mobile than those corresponding to the bulk. Focusing on the top left panel, we
 211 observe that in the bulk, and at low temperature, the distribution shows a vanishing
 212 probability for x -displacement larger than the near-neighbour distance ($x \sim 1$). As
 213 expected for a glassy behaviour, this implies that the particles have not managed to
 214 escape from the cages in which they were trapped initially. In contrast, the
 215 distribution for the top layer particles exhibits non-negligible values up to $x \sim 4$, thus
 216 providing evidence for an enhanced mobility at the free interface of the film. As
 217 expected, the difference between surface and bulk mobilities grows with time. Bulk

218 mobility remains practically unchanged at the timescales examined, since the system
 219 at the temperatures shown in Fig.2 resides below the estimated glass-transition
 220 temperature. Focusing on the top layer particles' distribution at early times, one can
 221 discern, apart from the peak at
 222 $x \sim 0.1$, the existence of a "shoulder" at distance $x \sim 1$. The distribution at later times
 223 further confirms the existence of two different populations, as reflected in the peaks at
 224 $x \sim 0.2$ and at $x \sim 1.1$. The appearance of these two peaks reflects a clear distinction in
 225 mobility for the surface and internal particles belonging to the top-layer and lies in
 226 accordance with the findings of Malshe et al.⁴². On the other hand, the distribution
 227 also shows that the peak belonging to the more mobile particles gains significantly in
 228 intensity as time lapses. This is consistent with the fact that an increasing fraction of
 229 the top-layer particles gets closer to the free surface with time (as demonstrated by the
 230 snapshots in Fig.1, blue particles).
 231 The previous two-peak fine-structure separation of relaxation processes is no longer
 232 detected at late times for $T > 0.30$, thus indicating a more homogenous mobility at
 233 higher temperature. Nevertheless, the "shoulder" observed in panels b and c at $x \sim 1$
 234 early times, is maintained and gains significantly in intensity at higher temperatures.
 235 Assuming that the mechanism of diffusion does not change appreciably at the sub-
 236 T_g temperatures examined, it is reasonable to surmise that this behavior arises from
 237 the same origin as in the lowest temperature case, *i.e.* the increase with time of the
 238 number of top-layer particles gaining access to the free surface. In sharp contrast,
 239 there is no sign of enhanced mobility in the bulk samples as temperature rises. Only at
 240 $T = 0.375$, one can discern a marginal increase in the mobility of the bulk particles at
 241 long times, as reflected by the tail of the van Hove distribution. Since the bimodal
 242 distribution at low temperatures which is indicative for the dynamic heterogeneity in
 243 the motion of the top layer particles, is no longer detected at elevated temperatures, it
 244 may be considered as a signature for the transition for these particles to the glassy
 245 state.
 246 To examine the global consequences of the enhanced surface mobility on the film
 247 leveling, we have monitored the average height $h_{av}(t)$ of the top layer particles. The
 248 initial value of h_{av} (counted from the substrate) was $h_{av0} = 13.5$. An example of the
 249 time evolution of the rescaled amplitude, $\frac{h_{av}(t)-h_{|v|}}{h_{av0}-h_{|v|}}$, for a temperature $T = 0.45$, is
 250 displayed in Fig.3a, where $h_{|v|} = 11.31$ is the average height of the top layer particles

251 after the film leveling. It should be noted here that $h_{|v|}$ is smaller than the value
 252 predicted from the volume conservation. This is due to the fact that, in this work, it is
 253 the average height of the square pattern that is monitored rather than its maximum
 254 height. On these grounds, $h_{|v|}$ does not correspond the value of $h_{av}(t)$ at infinite time
 255 and, consequently, it is not an equilibrium value. We stress that the total number of
 256 evaporated particles did not exceed 0.35% of the total number of particles constituting
 257 the film, for all simulated systems. As stated earlier, the evaporated particles were
 258 excluded from all analysis calculations. As it can be inferred from Fig.3a, the
 259 temporal decay is exponential. Figure 3b displays the associated decay constant as a
 260 function of temperature. We note that the minimum temperature at which full leveling
 261 of the square pattern was observed within the total simulation time, was $T = 0.30$.



262 Figure 3: a) Time evolution of the rescaled pattern amplitude at $T = 0.45$. The red line
 263 is an affine fit. b) Decay constant K extracted from the affine fits as a function of
 264 temperature. Error bars in K are on the order of 10^{-6} .

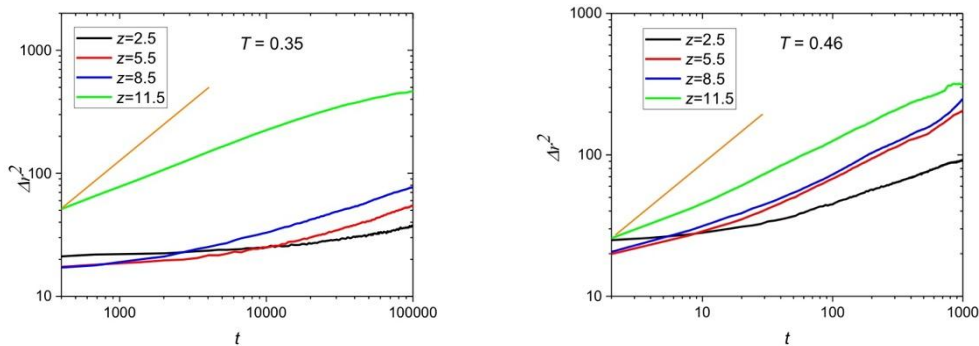
265

266 Examining Fig.3b, it appears that in between $T_g = 0.392$ and $T_c = 0.435$, a crossover
 267 takes place. At temperatures above T_c , a weak slope characteristic of a liquid-like
 268 behaviour is observed, while below T_g a stronger dependence corresponding to a
 269 glassy-like behaviour is noticed. This observation is consistent with the fact that the
 270 onset of supercooling effects is generally observed near T_c . Interestingly, recent
 271 experimental studies report different rates for the decay of patterned surfaces in
 272 supported films above and below the glass-transition temperature^{6, 9, 11, 13, 23}. The
 273 flattening of profile patterns at the free surface of films below T_g has been ascribed to
 274 surface diffusion as suggested by Mullin's theory¹⁹. It must be noted that, since the
 275 mobile layer can still be considered at equilibrium within a certain temperature range

276 below T_g , and thus the Stokes-Einstein relation is valid there, one can also describe
 277 the surface mobility as a surface flow which leads to an identical partial differential
 278 equation for the profile's evolution⁹. Surface diffusion levels a sinusoidal surface
 279 pattern at a decay rate proportional to q^4 , where q is the angular-wavenumber. Other
 280 mechanisms, such as bulk viscous flow and evaporation-condensation exhibit weaker
 281 q dependences (except for the limiting lubrication case⁹, that accidentally shows the
 282 same q^4 dependence for a bulk viscous flow above T_g). We have not investigated the
 283 angular- wavenumber dependence of the decay rate here but, instead, we have carried
 284 out a layer-resolved analysis of the particles' z -dependent mean-squared
 285 displacements (MSDs) as defined by:

$$\Delta r^2(z, t) = \left\langle \frac{1}{n_t} \sum_i |r_i(t) - r_i(0)|^2 \prod_{t'=0}^t \delta[z - z_i(t')] \right\rangle, \quad (2)$$

286 where $r_i(t)$ is the position of particle i at time t and $\langle \dots \rangle$ is an ensemble average. This
 287 definition takes into account only the n_t particles which are at all times $t' < t$ within
 288 the slab centred at z and bearing a width of $\Delta z = 1.5$. The results for the runs carried
 289 out at $T = 0.35$ are presented in Fig.4. For comparison purposes, the results for runs
 290 carried out above T_g , at $T = 0.46$, are also shown. We note here that the simulation
 291 runs at $T = 0.46$ were significantly shorter than the runs below T_g due to the
 292 evaporation of the surface particles.

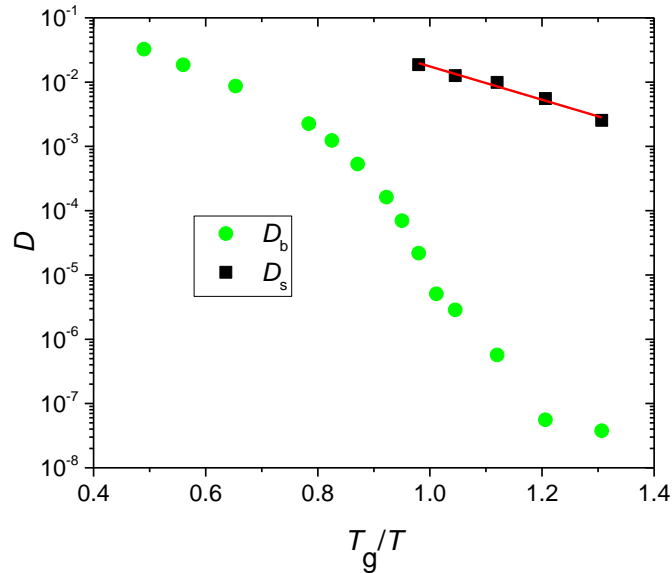


293 Figure 4: Layer-resolved mean-squared displacements (see eq.2) as a function of time,
 294 for various distances z from the substrate as indicated, and at temperatures a) $T = 0.35$
 295 and b) $T = 0.46$. Also shown in orange, is the scaling law $\Delta r^2 \sim t$.

296

297 Focusing on the left panel of Fig.4, it appears that, at $T = 0.35$, the MSD of the
 298 particles located in the outermost film layer near the film surface is about 5 times
 299 larger than the one for the particles in the second outermost film layer. There is no

300 sign of major propagation of the enhanced surface mobility into the bulk. This
 301 observation corroborates a scenario in which the relaxation of the square pattern is
 302 governed by surface diffusion below the glass transition. A similar behaviour was
 303 observed at all sampled temperatures below T_g . Furthermore, a visual inspection of
 304 the MSDs of the innermost particles (black lines in Fig.4), demonstrates enhanced
 305 dynamics near the solid substrate at short times. This behaviour lies in accordance
 306 with simulation studies of polymers near solid interfaces^{52,53,54}.
 307 Finally, the diffusion coefficients D_s of the top layer particles were extracted from the
 308 MSD curves at different temperatures, and compared with the corresponding bulk
 309 values, D_b in Fig.5.



310
 311 Figure 5: Diffusion coefficients of the top layer (D_s) and bulk (D_b) particles versus
 312 inverse temperature. The latter is scaled by the bulk T_g . The solid line is an affine fit
 313 in log-linear representation.

314
 315 As can be discerned, the diffusion coefficient of the top layer particles seems to
 316 exhibit an Arrhenius-type temperature dependence, which is reminiscent of previous
 317 observations for oligomer glasses^{6,9}. Moreover, diffusion at the surface is faster than
 318 in the bulk by a factor that ranges from 10^2 to 10^5 at the lowest temperature studied.
 319 This ratio drastically rises with cooling as it has been observed in both experimental
 320 and theoretical studies^{6,9,13,42}.

321

322 IV. Conclusion

323 Molecular dynamics simulations have been conducted in order to examine the decay
324 process of a periodic square-wave pattern at the free surface of a binary Lennard-
325 Jones film. Contrary to previous simulation studies of the capillary leveling of thin
326 films, the evolution of the height was examined over a wide temperature range
327 sampling both the liquid and glassy states of the film. Different mechanisms appeared
328 to control the pattern leveling in those two states. By the aid of layer-resolved analysis
329 of the particles' mean-squared displacements, we showed that diffusion is much more
330 efficient in the layer close to the free surface than elsewhere in the bulk. Specifically,
331 at the lowest temperature studied, the diffusion coefficient of the surface particles is
332 found to be 10^5 times larger than the bulk counterpart and this difference decreases
333 upon heating.

334

335 **Acknowledgements**

336 The authors gratefully acknowledge financial support from ANR WAFPI and ANR
337 FSCF, as well as the Global Station for Soft Matter, a project of Global Institution for
338 Collaborative Research and Education at Hokkaido University. Hendrik Meyer is
339 kindly thanked for providing the layer-resolved analysis code. The authors also thank
340 Anthony Maggs, Elie Raphaël, Kari Dalnoki-Veress, James Forrest, Joshua McGraw,
341 Oliver Bäümchen and Jörg Baschnagel for stimulating discussions. K.K. would like to
342 thank FO.R.TH.-IESL for the warm hospitality during his stay there.

343

344 **References**

- 345 (1) Ulbricht, M. Advanced functional polymer membranes. *Polymer* **2006**, *47*,
346 2217-2262.
- 347 (2) Hasebe, M.; Musumeci, D.; Powell, C. T.; Cai, T.; Gunn, E.; Zhu, L.; Yu, L.
348 Fast surface crystal growth on molecular glasses and its termination by the onset of
349 fluidity. *J. Phys. Chem. B* **2014**, *118*, 7638-7646.
- 350 (3) Sun, Y.; Zhu, L.; Kearns, K. L.; Ediger, M. D.; Yu, L. Glasses crystallize
351 rapidly at free surfaces by growing crystals upward. *Proc. Natl. Acad. Sci. U.S.A.*
352 **2011**, *108*, 5990-5995.
- 353 (4) Ediger, M. D. Vapor-deposited glasses provide clearer view of two-level
354 systems. *Proc. Natl. Acad. Sci. U.S.A.* **2014**, *111*, 11232-11233.

- 355 (5) Mangalara, J. H.; Marvin, M. D.; Simmons, D. S. Three-layer model for the
356 emergence of ultrastable glasses from the surfaces of supercooled liquids. *J. Phys.*
357 *Chem. B* **2016**, *120*, 4861-4865.
- 358 (6) Yang, Z.; Fujii, Y.; Lee, F. K.; Lam, C.-H.; Tsui, O. K. C. Glass transition
359 dynamics and surface layer mobility in unentangled polystyrene films. *Science* **2010**,
360 *328*, 1676-1679.
- 361 (7) Yang, Z.; Clough, A.; Lam, C.-H.; Tsui, O. K. C. Glass transition dynamics
362 and surface mobility of entangled polystyrene films at equilibrium. *Macromolecules*
363 **2011**, *44*, 8294-8300.
- 364 (8) Mapes, M. K.; Swallen, S. F.; Ediger, M. D. Self-diffusion of supercooled o-
365 terphenyl near the glass transition temperature. *J. Phys. Chem. B* **2006**, *110*, 507-511.
- 366 (9) Chai, Y.; Salez, T.; McGraw, J. D.; Benzaquen, M.; Dalnoki-Veress, K.;
367 Raphaël, E.; Forrest, J. A. A direct quantitative measure of surface mobility in a
368 glassy polymer. *Science* **2014**, *343*, 994-999.
- 369 (10) Teisseire, J.; Revaux, A.; Foresti, M.; Barthel, E. Confinement and flow
370 dynamics in thin polymer films for nanoimprint lithography. *Appl. Phys. Lett.* **2011**,
371 *98*, 013106.
- 372 (11) Fakhraai, Z.; Forrest, J. A. Measuring the surface dynamics of glassy
373 polymers. *Science* **2008**, *319*, 600.
- 374 (12) Zhang, W.; Yu, L. Surface diffusion of polymer glasses. *Macromolecules*
375 **2016**, *49*, 731-735.
- 376 (13) Brian, C. W.; Yu, L. Surface self-diffusion of organic glasses. *J. Phys. Chem.*
377 *A* **2013**, *117*, 13303-13309.
- 378 (14) Hamdorf, M.; Johannsmann, D. Surface-rheological measurements on glass
379 forming polymers based on the surface tension driven decay of imprinted corrugation
380 gratings. *J. Chem. Phys.* **2000**, *112*, 4262-4270.
- 381 (15) Zhang, W.; Brian, C. W.; Yu, L. Fast surface diffusion of amorphous o-
382 terphenyl and its competition with viscous flow in surface evolution. *J. Phys. Chem. B*
383 **2015**, *119*, 5071-5078.
- 384 (16) Ruan, S.; Musumeci, D.; Zhang, W.; Gujral, A.; Ediger, M. D.; Yu, L. Surface
385 transport mechanisms in molecular glasses probed by the exposure of nano-particles.
386 *J. Chem. Phys.* **2017**, *146*, 203324.

- 387 (17) Kim, H.; Rühm, A.; Lurio, L. B.; Basu, J. K.; Lal, J.; Lumma, D.; Mochrie, S.
388 G. J.; Sinha, S. K. Surface dynamics of polymer films. *Phys. Rev. Lett.* **2003**, *90*,
389 068302.
- 390 (18) Wang, L.; Ellison, A. J. G.; Ast, D. G. Investigation of surface mass transport
391 in Al–Si–Ca–oxide glasses via the thermal induced decay of submicron surface
392 gratings. *J. Appl. Phys.* **2007**, *101*, 023530.
- 393 (19) Mullins, W. W. Flattening of a nearly plane solid surface due to capillarity. *J.*
394 *Appl. Phys.* **1959**, *30*, 77-83.
- 395 (20) Bonzel, H. P.; Latta, E. E. Surface self-diffusion on Ni(110): Temperature
396 dependence and directional anisotropy. *Surf. Sci.* **1978**, *76*, 275-295.
- 397 (21) Keeffe, M. E.; Umbach, C. C.; Blakely, J. M. Surface self-diffusion on Si from
398 the evolution of periodic atomic step arrays. *J. Phys. Chem. Solids* **1994**, *55*, 965-973.
- 399 (22) Zhu, L.; Brian, C. W.; Swallen, S. F.; Straus, P. T.; Ediger, M. D.; Yu, L.
400 Surface self-diffusion of an organic glass. *Phys. Rev. Lett.* **2011**, *106*, 256103.
- 401 (23) Chen, Y.; Zhang, W.; Yu, L. Hydrogen bonding slows down surface diffusion
402 of molecular glasses. *J. Phys. Chem. B* **2016**, *120*, 8007-8015.
- 403 (24) Donati, C.; Glotzer, S. C.; Poole, P. H.; Kob, W.; Plimpton, S. J. Spatial
404 correlations of mobility and immobility in a glass-forming Lennard-Jones liquid.
405 *Phys. Rev. E* **1999**, *60*, 3107-3119.
- 406 (25) Kob, W.; Donati, C.; Plimpton, S. J.; Poole, P. H.; Glotzer, S. C. Dynamical
407 heterogeneities in a supercooled Lennard-Jones liquid. *Phys. Rev. Lett.* **1997**, *79*,
408 2827-2830.
- 409 (26) Andersen, H. C. Molecular dynamics studies of heterogeneous dynamics and
410 dynamic crossover in supercooled atomic liquids. *Proc. Natl. Acad. Sci. U.S.A.* **2005**,
411 *102*, 6686-6691.
- 412 (27) Kob, W. Computer simulations of supercooled liquids and glasses. *J. Phys.*
413 *Condens. Matter* **1999**, *11*, R85.
- 414 (28) Murthy, S. S. N. Molecular dynamics in supercooled liquids: A study of the
415 relaxation in binary solutions. *J. Mol. Liq.* **1992**, *51*, 197-217.
- 416 (29) Pakula, T. Collective dynamics in simple supercooled and polymer liquids. *J.*
417 *Mol. Liq.* **2000**, *86*, 109-121.
- 418 (30) Vogel, M.; Medick, P.; Rossler, E. Slow molecular dynamics in binary
419 organic glass formers. *J. Mol. Liq.* **2000**, *86*, 103-108.

- 420 (31) Hocky, G. M.; Berthier, L.; Kob, W.; Reichman, D. R. Crossovers in the
421 dynamics of supercooled liquids probed by an amorphous wall. *Phys. Rev. E* **2014**,
422 89, 052311.
- 423 (32) Scheidler, P.; Kob, W.; Binder, K. Cooperative motion and growing length
424 scales in supercooled confined liquids. *EPL Europhys. Lett.* **2002**, 59, 701.
- 425 (33) Varnik, F.; Scheidler, P.; Baschnagel, J.; Kob, W.; Binder, K. Molecular
426 dynamics simulation of confined glass forming liquids. *Mater. Res. Soc. Symp. Proc.*
427 **2000**, 651, T3.1.1.
- 428 (34) Scheidler, P.; Kob, W.; Binder, K. The relaxation dynamics of a simple glass
429 former confined in a pore. *EPL Europhys. Lett.* **2000**, 52, 277.
- 430 (35) Scheidler, P.; Kob, W.; Binder, K. The relaxation dynamics of a supercooled
431 liquid confined by rough walls. *J. Phys. Chem. B* **2004**, 108, 6673-6686.
- 432 (36) Singh, S.; Ediger, M. D.; de Pablo, J. J. Ultrastable glasses from in silico
433 vapour deposition. *Nat. Mater.* **2013**, 12, 139.
- 434 (37) Lin, P.-H.; Lyubimov, I.; Yu, L.; Ediger, M. D.; de Pablo, J. J. Molecular
435 modeling of vapor-deposited polymer glasses. *J. Chem. Phys.* **2014**, 140, 204504.
- 436 (38) Marcos, F. C.; Ezequiel, V. A. Continuous and discrete modeling of the decay
437 of two-dimensional nanostructures. *J. Phys. Condens. Matter* **2009**, 21, 263001.
- 438 (39) Kayhani, K.; Mirabbaszadeh, K.; Nayebi, P.; Mohandesi, A. Surface effect on
439 the coalescence of Pt clusters: A molecular dynamics study. *Applied Surf. Sci.* **2010**,
440 256, 6982-6985.
- 441 (40) Hoang, V. V.; Dong, T. Q. Free surface effects on thermodynamics and glass
442 formation in simple monatomic supercooled liquids. *Phys. Rev. B* **2011**, 84, 174204.
- 443 (41) Haji-Akbari, A.; Debenedetti, P. G. The effect of substrate on thermodynamic
444 and kinetic anisotropies in atomic thin films. *J. Chem. Phys.* **2014**, 141, 024506.
- 445 (42) Malshe, R.; Ediger, M. D.; Yu, L.; de Pablo, J. J. Evolution of glassy gratings
446 with variable aspect ratios under surface diffusion. *J. Chem. Phys.* **2011**, 134, 194704.
- 447 (43) Kuon, N.; Flenner, E.; Szamel, G. Comparison of single particle dynamics at
448 the center and on the surface of equilibrium glassy films. *J. Chem. Phys.* **2018**, 149,
449 074501.
- 450 (44) Tanis, I.; Meyer, H.; Salez, T.; Raphaël, E.; Maggs, A. C.; Baschnagel, J.
451 Molecular dynamics simulation of the capillary leveling of viscoelastic polymer films.
452 *J. Chem. Phys.* **2017**, 146, 203327.

453 (45) Kob, W.; Andersen, H. C. Testing mode-coupling theory for a supercooled
454 binary Lennard-Jones mixture. *Transport Theor. Stat. Phys.* **1995**, *24*, 1179-1198.

455 (46) Kob, W.; Barrat, J.-L. Aging effects in a Lennard-Jones glass. *Phys. Rev. Lett.*
456 **1997**, *78*, 4581-4584.

457 (47) Li, R.; Wang, L.; Yue, Q.; Li, H.; Xu, S.; Liu, J. Insights into the adsorption of
458 oxygen and water on low-index Pt surfaces by molecular dynamics simulations. *New*
459 *J. Chem.* **2014**, *38*, 683-692.

460 (48) Smith, W.; Todorov, I. T. A short description of DL_POLY. *Mol. Simul.*
461 **2006**, *32*, 935-943.

462 (49) Youngs, T. G. A. Aten—An application for the creation, editing, and
463 visualization of coordinates for glasses, liquids, crystals, and molecules. *J. Comput.*
464 *Chem.* **2009**, *31*, 639-648.

465 (50) Kob, W.; Andersen, H. C. Scaling behavior in the beta-relaxation regime of a
466 supercooled Lennard-Jones mixture. *Phys. Rev. Lett.* **1994**, *73*, 1376-1379.

467 (51) Humphrey, W.; Dalke, A.; Schulten, K. VMD: Visual molecular dynamics, *J.*
468 *Mol. Graph.* **1996**, *14*, 33-38.

469 (52) Daoulas, K. C.; Harmandaris, V. A.; Mavrantzas, V. G. Molecular dynamics
470 simulation of a polymer melt/solid interface: local dynamics and chain mobility in a
471 thin film of polyethylene melt adsorbed on graphite. *Macromolecules* **2005**, *38*, 5796–
472 5809.

473 (53) Kritikos, G.; Sgouros, A.; Vogiatzis, G. G.; Theodorou, D. N. Molecular
474 dynamics study of polyethylene under extreme confinement. *J. Phys. Conf. Ser.* **2016**,
475 *738*, 012012.

476 (54) Baschnagel, J.; Binder, K.; Milchev, A. Mobility of polymers near surfaces. In
477 *Polymer Surfaces, Interfaces and Thin Films* **2000**, 1–49.

478
479
480
481
482
483
484
485
486

487

488

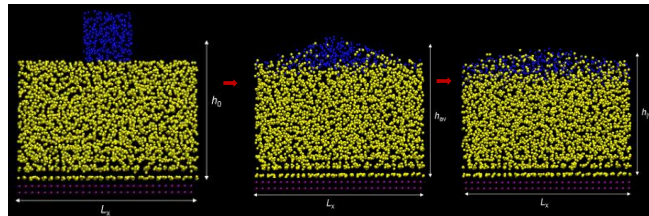
489

490

491

492

TOC Graphic



493